Dynamical environments of MU69 and similar objects

Guillaume Rollin[a,*], Ivan I. Shevchenko[b], José Lages[a]

[a] *Institut UTINAM, Observatoire des Sciences de l'Univers THETA, CNRS, Université Bourgogne Franche-Comté, Besançon 25030, France*
[b] *Saint Petersburg State University, 7/9 Universitetskaya nab., 199034 Saint Petersburg, Russia*

Abstract

We explore properties of the long-term dynamics of particles (moonlets, fragments, debris etc.) around KBO 2014 MU69 (Arrokoth), as well as around similar contact-binary objects potentially present in the Kuiper belt. The chaotic diffusion of particles inside the Hill sphere of MU69 (or, generally, a similar object) is studied by means of construction of appropriate stability diagrams and by application of analytical approaches generally based on the Kepler map theory. The formation and evolution of the particle clouds, due to the chaotic diffusion inside the Hill sphere, are studied and the cloud lifetimes are estimated.

Keywords: celestial mechanics, dynamical chaos, contact binaries, Kuiper belt objects, 2014 MU69, Arrokoth

1. Introduction

The second (after Pluto) target object for the New Horizons mission was chosen in 2014, finalizing an observation survey performed with the Hubble Space Telescope (Stern, 2017). It was called 2014 MU69, and, subsequently, (486958) Arrokoth (temporarily it was also nicknamed Ultima Thule). Later on, due to results of dedicated observational campaigns (Stern, 2017; Parker et al., 2017), this object was suspected to be a classical KBO, a primordial contact binary (hereafter CB). A dumbbell contact-binary shape is typical for KBOs.

*Corresponding author
Email addresses: guillaume.rollin@utinam.cnrs.fr (Guillaume Rollin), i.shevchenko@spbu.ru (Ivan I. Shevchenko), jose.lages@utinam.cnrs.fr (José Lages)

However, up to the time of the New Horizons flyby, its lightcurve monitoring had not succeeded to retrieve the rotation period, because visual magnitude variations were unresolved (Benecchi, 2016).

The rendezvous of New Horizons and Arrokoth took place on January 1, 2019. Indeed, Arrokoth turned out to be a contact binary (Stern et al., 2019; Cheng et al., 2019; Protopapa et al., 2019; Stern et al., 2019), visually fitting a dumbbell model, depicted, e.g., in Fig. 5 in Scheeres (2007), or most similar, in Fig. 1 in Lages, Shepelyansky & Shevchenko (2017).[1] Tantalizingly, the ratio of masses of the binary components has turned out to be $\sim 1/3$, very similar to the ratios typical for contact-binary cometary nuclei, as compiled in Table 1 in Lages, Shevchenko & Rollin (2018).

Identifying any material in the vicinities of a target object of a space mission is of an especial concern for planning cosmic flybys, including that by Arrokoth (Moore et al., 2018), as the material is hazardous for a space probe. Low-mass shallow matter orbiting around Arrokoth, as around any other KBO, may originate from a number of processes. It may be left from a primordial swarm of solids (McKinnon et al., 2019), or it may be ejecta of various origins: ejecta due to early out-gassing (Thomas et al., 2015; Shao & Lu, 2000); ejecta from impacting by intruding bodies (Nesvorný et al., 2018); ejecta resulting from the CB-forming collision (Umurhan et al., 2019). However, up to now, no moons, moonlets, fragments, or debris (Kammer et al., 2018; Spencer et al., 2019, 2020), or any traces of coma (Gladstone et al., 2019), have been discerned in not-yet-completed image surveys, performed from HST and New Horizons in the field around Arrokoth.

As shown in Lages & Shevchenko (2020), based on preliminary data on the shape of Arrokoth, this rotating CB is able to efficiently cleanse its vicinities by chaotizing all material orbiting it sufficiently close. In this article, we explore properties of the long-term dynamics of low-mass matter (whatever it can be: moonlets, fragments etc.) around CB-shaped objects, expected to be ubiquitous

[1] Later on, the Arrokoth constituents were reported to be flattened (Stern et al., 2019).

in the Kuiper belt.

To assess a global picture of the dynamical environment of Arrokoth or a similar object, it is necessary (1) to analyze the process of cleansing of the circum-binary chaotic zone; (2) to analyze the process of formation and further survival of a cocoon, formed by the ejected matter inside CB's Hill sphere. In this article, our study is concentrated on just these two items. Therefore, we are interested in the timescale of clearing the immediate vicinity of Arrokoth (the chaotic circum-binary zone), the possibility and timescale of formation of a cocoon of ejected matter around Arrokoth inside its Hill sphere, and the survivability of such a cocoon.

In our study, we aim to assess the rate of clearing process in the chaotic circumbinary zone; to obtain the mass parameter dependence of the depopulation rate; to estimate the characteristic time of dispersal of low-mass matter out from Arrokoth's Hill sphere, if such matter were initially present; to assess collisional hazards for space probes visiting neighborhoods of Arrokoth-like objects in the Kuiper belt.

2. Circum-CB clearing: the problem setting

Spinning gravitating CB-shaped bodies create zones of dynamical chaos around them (Lages, Shepelyansky & Shevchenko, 2017), and this has a clearing effect: any material put in orbits around a rotating dumbbell (e.g., any material ejected from its surface) cannot survive in this chaotic zone. It either escapes into space, or is absorbed by the parent body's surface (Lages, Shevchenko & Rollin, 2018). As the orbiting matter is removed in this way, a spinning gravitating CB cleans-up its vicinities.

A much more well-known example of analogous "cleansing" is the formation of the gap in the close-to-coorbital neighbourhood of a planet (Wisdom, 1980; Duncan, Quinn, & Tremaine, 1989; Morrison & Malhotra, 2015). The close-to-coorbital chaotic gap is formed by the overlap of the first-order mean-motion resonances accumulating in the neighbourhood of a planet's orbit; whereas the

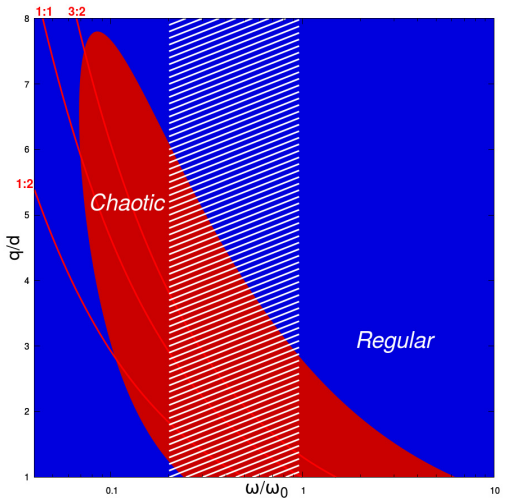

Figure 1: Extents of the chaotic zone (shown in red) around a contact binary as a function of the binary's rotation rate ω, in ratio to the critical ω_0. The pericentric distance q is measured in units of d, the contact binary size. White shaded area delimits the range of typical rotation rates of the Kuiper belt objects, according to data in Thirouin et al. (2014). Red solid curves show locations of three major spin-orbit resonances.

circum-CB chaotic zone is formed by the overlap of the accumulating integer spin-orbit resonances with the rotating dumbbell (Lages, Shevchenko & Rollin, 2018). In the both cases, any material injected into the chaotic zones is subject to an unlimited chaotic diffusion in the eccentricity (as well as subject to possible close encounters with the CB or the planet) and, therefore, finally is removed.

In Fig. 1, adapted from our previous study (Lages, Shevchenko & Rollin, 2018), we represent graphically the extents of the circum-CB chaotic zone. The diagram is set in the "CB rotation rate – particle's initial pericentric distance" frames. The rotation rate ω is measured in units of its critical value ω_0, corresponding to centrifugal disintegration of the initially-contact binary (ω_0 is equal to CB's Keplerian rate of rotation). The pericentric distance q is in units of the binary's size d, defined as the distance between the mass centers of its components. In units of the critical rate ω_0, the typical rotation rates ω of the Kuiper belt objects range from 0.2 to 1 (thus, the periods range from 1 to 5, in

critical periods), according to the observational (lightcurve) data given in Thirouin et al. (2014). The area bounded by these limits in Fig. 1 is white-shaded. Locations of main resonances 1:2, 1:1, and 3:2 between orbiting particles and the rotating central body are shown as red curves. Fig. 1 demonstrates that typical Kuiper belt CBs may have rather extended circum-body chaotic zones: for orbits inside such zones, the initial pericentric distance q ranges up to $\sim 6d$.

Recall that the radius of a gravitating body's Hill sphere $R_{\rm H}$, in units of the semimajor axis of a perturber, a_0, is given by

$$\frac{R_{\rm H}}{a_0} = \left(\frac{m}{3M}\right)^{1/3}, \tag{1}$$

where M and m are the primary's and secondary's masses, respectively (those of the Sun and Arrokoth, in our problem). The orbit of Arrokoth's any moonlet should lie within Arrokoth's Hill sphere. This implies the inequality $a(1+e) \lesssim R_{\rm H}$.

Given the "dumbbell size" of Arrokoth $d \simeq 17$ km (Stern et al., 2019; McKinnon, 2020), it is straightforward to estimate, using the diagram, that the chaotic clearing zone around Arrokoth may have radius of at most ∼100 km, an order of magnitude less than the New Horizons flyby distance (∼3500 km) and three orders of magnitude less than Arrokoth's Hill radius ($\sim 5 \cdot 10^4$ km).

3. Numerical simulations: the stability diagram

To describe the immediate dynamical environments of Arrokoth, we construct stability charts in the q–e (pericentric distance – eccentricity) plane of initial conditions. We use the Lyapunov characteristic exponent (LCE) method, that we have earlier employed in Lages, Shepelyansky & Shevchenko (2017); Lages, Shevchenko & Rollin (2018). We choose an inertial Cartesian coordinate system with the origin at the CB's center of mass. The equations of motion of

the particle with coordinates (x, y) are given by

$$\begin{aligned}
\dot{x} &= v_x, \\
\dot{y} &= v_y, \\
\dot{v}_x &= -\frac{m_2\,(x-x_2)}{\left((y-y_2)^2+(x-x_2)^2\right)^{3/2}} - \frac{m_1\,(x-x_1)}{\left((y-y_1)^2+(x-x_1)^2\right)^{3/2}}, \\
\dot{v}_y &= -\frac{m_2\,(y-y_2)}{\left((y-y_2)^2+(x-x_2)^2\right)^{3/2}} - \frac{m_1\,(y-y_1)}{\left((y-y_1)^2+(x-x_1)^2\right)^{3/2}},
\end{aligned} \tag{2}$$

where (x_1, y_1) and (x_2, y_2) are the coordinates of the centers of masses m_1 and m_2, respectively. The locations x_1, y_1 and x_2, y_2 of the primaries are given by

$$\begin{aligned}
x_1 &= \mu\cos(\omega t), \\
y_1 &= \mu\sin(\omega t), \\
x_2 &= (\mu-1)\cos(\omega t), \\
y_2 &= (\mu-1)\sin(\omega t).
\end{aligned} \tag{3}$$

The quantity ω is a parameter responsible for the arbitrary rotation frequency of the CB; ω is equal to CB's rotation rate in units of its critical rotation rate corresponding to centrifugal disintegration. At $\omega = 1$, the equations reduce to the usual equations of motion in the planar restricted three-body problem. The distance between the centers of masses m_1 and m_2 is set here to unity, $d = 1$. Also we set $\mathcal{G}(m_1 + m_2) = 1$; therefore, the angular rate of the Keplerian orbital motion of the binary (if it were unbound) is

$$\omega_0 = \left(\mathcal{G}(m_1 + m_2)/d^3\right)^{1/2} = 1.$$

Arrokoth constitutes an alliance of two round bodies[2]; therefore, the dynamical model given by Equations (2)–(3) is expected to be essentially adequate.

We set the physical and dynamical parameters of Arrokoth as obtained during the New Horizons flyby (Stern et al., 2019; Cheng et al., 2019; Protopapa et al., 2019; Stern et al., 2019).

[2] Although flattened; but as soon as the Arrokoth components are flattened mostly orthogonal to its rotation plane (McKinnon, 2020), this flattening does not compromise our dumbbell model for the gravitational potential.

A two-mascon model for Arrokoth shape model, with the parameters as given in Stern et al. (2019) and McKinnon (2020) provides us with the following data.

- The "dumbbell size" of Arrokoth (the distance between the centers of masses m_1 and m_2: $d = 17.2$ km and the radii of the components $R_1 \approx 10.1$ km, $R_2 \approx 7.3$ km.
- Masses, assuming a typical density $\rho = 0.5$ g/cm^3 for cometary nuclei: $m_1 = 1.01 \cdot 10^{18}$ g and $m_2 = 5.45 \cdot 10^{17}$ g. Therefore, $m_1/m_2 = 1.85$ and the reduced mass of the contact binary $\mu \equiv m_2/(m_1 + m_2) = 0.35$.
- Rotation period of Arrokoth: $P_{\rm rot} = 15.92$ h, therefore $\omega = 0.77$.

The initial conditions and technical parameters are as follows:

- the initial positions of the two masses are set along the x axis,
- the initial position of the test particle is at the pericenter and its initial velocity vector (calculated in the Arrokoth–particle two-body model) is orthogonal to the x axis,
- the maximum computation time $T_{\rm max} = \omega \times 10^5$, in Arrokoth's rotation periods, is set in computations of the stability diagrams; and $T_{\rm max} = 10^5$, in Arrokoth's rotation periods, is set in computations of the ejection statistics.

To build the stability diagram, 200×200 orbits were computed using the Dormand–Prince integrator DOP853 (Hairer et al., 1987). The local error tolerance of the integrator was set to 10^{-10}. The code makes a loop over N_e initial values of eccentricity e for any fixed initial pericentric distance q. A *Python* code generates $N_q = 200$ executables with various values of q. Thus, their total number is 200.

The constructed LCE diagram of the global dynamics immediately around Arrokoth is shown in Fig. 2. The most prominent feature of this diagram is the

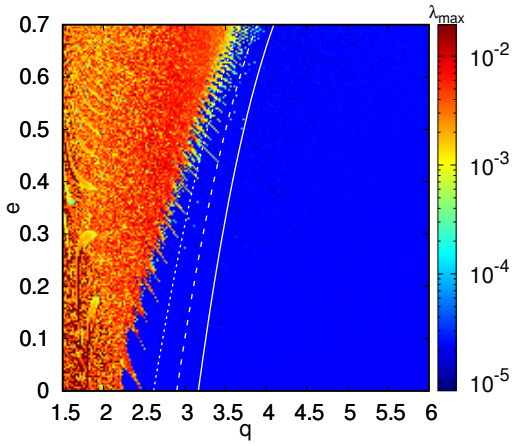

Figure 2: The LCE stability diagram of the immediate dynamical environments of Arrokoth, in finite-time LCE colour gradation.

"ragged" border between the circumbinary chaotic zone and the outer region of regular motion. The border is formed by the overlap of spin-orbit resonances between the rotating Arrokoth and an orbiting particle. The most prominent "teeth" of instability visible in Fig. 2 correspond to integer ratios of Arrokoth's rotation rate and an orbiting particle's mean motion, i.e., to the $p/1$ spin-orbit resonances.

Let K be the stochasticity parameter, characterizing the overlap of the integer spin-orbit resonances locally in the phase space of motion, as defined in Lages, Shevchenko & Rollin (2018). In Fig. 2, the solid white curves are the theoretical borders (taking place at the critical value $K_{\rm G} = 0.971635406$) between the chaotic and regular zones; the dashed curves are for $K = 2$; and the short-dashed curves are for $K = 4$. These theoretical borders are given by Equations (6) and (11) in Lages, Shevchenko & Rollin (2018). One may see that the numerically revealed borders of chaos generally agree with the analytical predictions: indeed, the $K = 4$ analytical curve serves approximately as a borderline above which the chaos is complete, i.e., any regular component is negligible.

In Fig. 3, additional diagrams are constructed by means the "movable LCE

distribution peaks" technique. This technique allows one to sharply separate chaotic orbits from regular ones instead of analyzing any continuous gradation of orbits in calculated finite-time LCE values; see Shevchenko & Melnikov (2003) for the technique description and details.

In Fig. 3, the panel (a) corresponds to the current (contact-binary) state of Arrokoth with the following parameters: $\mu \simeq 0.35$ and $\omega = 0.77$. We still see the properties described above: the "ragged" border and the most prominent "teeth" of instability corresponding to integer ratios of Arrokoth's rotation rate and the orbiting particle's mean motion. For circular orbits ($e = 0$), the chaos zone size is $\simeq 2.5$ times greater than the distance between the two masses. The panel (b) is for a non-contact pre-merger phase; here $\omega = 1$. Unlike the panel (a), the chaos zone size is now $\simeq 2$ times greater than the distance between the two masses for the circular orbits. In the both panels, the solid white curves are the theoretical borders between chaotic and regular zones at $K = K_{\rm G} \simeq 0.971635406$, the dashed curves are built at $K = 2$, and the short-dashed curves at $K = 4$. The theoretical borders are constructed as in Fig. 2.

Implications of the obtained diagrams are discussed further on in the following Sections.

4. General background and assumptions

Generally, the Fokker–Planck formalism can be used (adapting approaches proposed in Murray & Holman 1997, Section 3.4, and in Tremaine 1993; see also Duncan, Quinn, & Tremaine 1987; Malyshkin & Tremaine 1999) to obtain analytical estimates of the diffusion rates in clearing processes in such or similar systems. Here we base on the modified Kepler map theory, as developed in Lages, Shepelyansky & Shevchenko (2017); Lages, Shevchenko & Rollin (2018) (see also a review in Lages, Shepelyansky & Shevchenko 2018) to describe chaotic dynamical environments of rotating CBs.

It is important to note that our analysis is mostly developed in the assumption that the rotation rate ω of the contact binary is approximately the

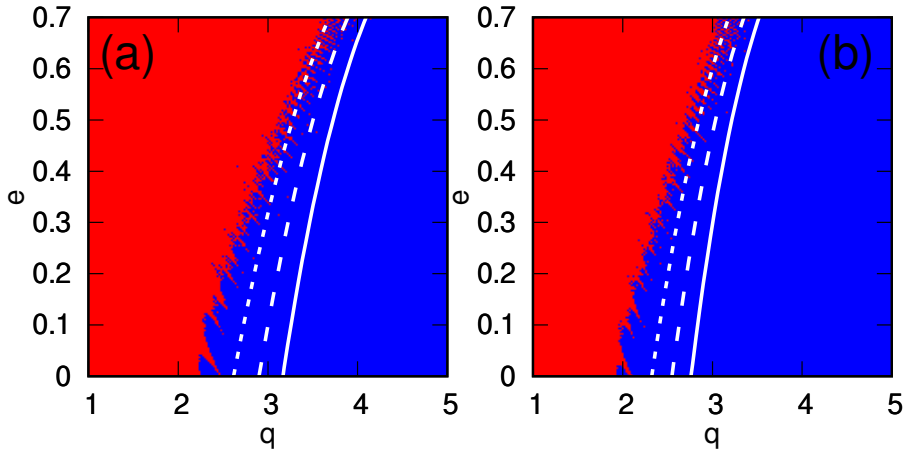

Figure 3: LCE stability diagrams for the current and pre-merger states of Arrokoth; red and blue colors correspond to chaotic and regular orbits, respectively. Left panel (a) is for the contact-binary phase, and right panel (b) is for a pre-merger phase of this KBO; see text for details.

same as its critical rotation rate ω_0 of centrifugal disintegration; i.e., $\omega \sim \omega_0$. For Arrokoth, $\omega \simeq 0.6\omega_0$ (assuming the typical density $\rho = 0.5$ g/cm^3; for smaller densities ω would be more close to unity). This assumption allows one to straightforwardly apply formulas already known for the case of motion around Keplerian binaries, without any their modification. As soon as the physical inferences made below do not mostly require any estimates to be accurate better than by an order of magnitude, we believe that the assumption $\omega \sim \omega_0$ is plausible for our purposes.

In accord with the general scenarios of formation of contact binaries in the Kuiper belt (Umurhan et al., 2019; McKinnon et al., 2019), we assume that, in the post-formation phase of Arrokoth's evolution, the particles initially reside in a disk-like structure around the merged binary. The theoretical circum-CB chaotic zone in this disk may extend up to radii $\simeq 6d$, as follows from Figs. 1 and 2.

In accord with the Kepler map theory basics, we assume that, in the motion of particles, the pericentric distance q is approximately conserved, while the

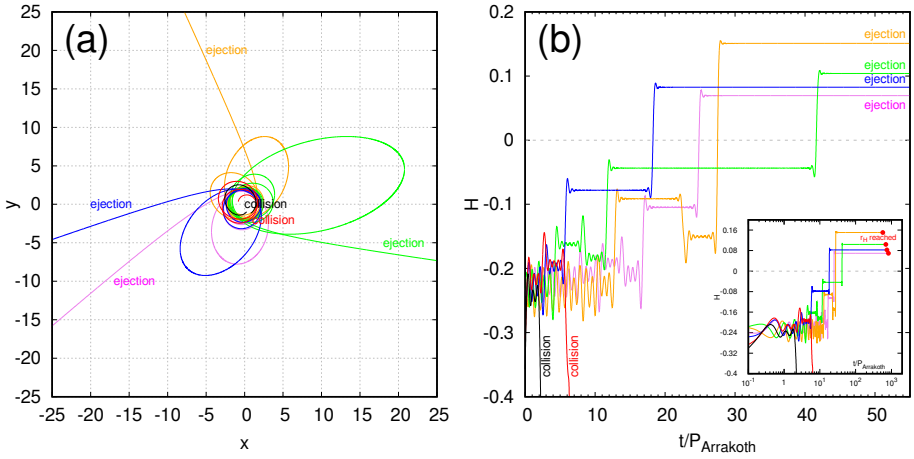

Figure 4: Examples of trajectories and time evolutions of their energies. Left panel (a): trajectories with the initial pericentric distance $q \simeq 1.40$ (black curve), $q \simeq 1.80$ (red), $q \simeq 2.13$ (blue), $q \simeq 2.19$ (green), $q \simeq 2.23$ (orange) and $q \simeq 2.27$ (purple); the initial eccentricity $e = 0$ in all cases. Right panel (b): time evolutions of the quantity $H = 2|E|$ for the trajectories presented in panel (a); the curves are coloured accordingly. The close-up: the H evolutions with time in a greater range, until the particles cross the Hill radius; the crossings are marked with red dots.

semimajor axis is subject to random walk (see Shevchenko 2011, 2015). The constancy of q seems plausible down to its values of $\sim 2d$; at smaller q, the employed approximations become more and more approximate; in particular, mergers of particles with Arrokoth become prevalent, thus removing them. We should outline that once q (which is greater than d) is assumed to be constant, no collisions with Arrokoth are possible theoretically; therefore, the collisions are generally ignored in what follows.

To illustrate that the chaotic dynamics of particles until they reach the Hill sphere border does indeed have a diffusive character, in Fig. 4 we present examples of trajectories and time evolutions of their energies. In panel (a), trajectories are shown with various initial pericentric distances q; the initial eccentricity $e = 0$ in all cases. In panel (b), time evolutions of the energies of the same trajectories are given (the curves are coloured accordingly). The close-up shows the quantity $H = 2|E|$ (where the energy $E = -1/(2a)$, and a

is the particle's orbital semimajor axis) evolutions with time in a greater range, until the particles cross the Hill radius; the crossings are marked with red dots. One may see that, for non-collisional cases, the orbital evolution of the particles has a random walk character (i.e., a chaotical diffusive character) in the energy, and, therefore, in semimajor axis as well.

5. Dispersal of matter around CBs

For any kind of discrete motion, the diffusion coefficient D can be defined, formally, as the mean-square spread in a selected variable (say, H), per time unit:

$$D_H \equiv \lim_{t\to\infty} \frac{\langle (H_t - H_0)^2 \rangle}{t}, \tag{4}$$

where t is time, the angular brackets denote averaging over a set of starting values (see, e.g., Meiss 1992).

Let us define the quantity $H = 2|E|$, where the energy $E = -1/(2a)$, and a is the particle's orbital semimajor axis; and the central binary's mass parameter $\mu \equiv m_2/(m_1 + m_2)$. We extrapolate a numerical-experimental expression, presented in Duncan, Quinn, & Tremaine (1987) for the rate of diffusion of circumbinary particles, from small to moderate values of μ. Taking into account that the rotation rates of the Kuiper belt CBs, including Arrokoth, are normally of the order of the critical rate of centrifugal disintegration (as already assumed above), one has

$$D_H \simeq 100\, H^2 \mu^2, \tag{5}$$

where time is measured in pericenter passages.

For the diffusion timescale, defined as the time needed for the particle's energy to change by an order of unity, one has

$$T_\mathrm{d} \simeq P \frac{H^2}{D_H} \simeq 0.01 \mu^{-2} P, \tag{6}$$

where P is the particle's orbital period averaged over the chaotic zone.

We take $P \simeq 2\pi a^{3/2}/(\mathcal{G}m_{\rm CB})^{3/2}$, where $a \sim 5d$, and d is the CB's size in the mascon model. Then, from Equation (6) one may directly see that for a CB like Arrokoth (with $\mu \sim 0.1$–0.3) the characteristic timescale of the diffusion in the CB's chaotic dynamical environment can be as small as ~ 10 times its rotation period; therefore, the clearing of the chaotic zone is, in fact, practically instantaneous.

Although our estimate of the transport time has been made in the diffusional approximation, its smallness verifies that, actually, this approximation is invalid and the transport is not diffusional, but ballistic: the clearing process is almost "single-kick." This can be shown independently by calculating the amplitude of the kick function in the Kepler map theory for CBs, presented in Lages, Shepelyansky & Shevchenko (2017); Lages, Shevchenko & Rollin (2018); the kick function in the normalized energy is given by

$$\Delta E\left(\mu, q, \omega, \phi\right) \simeq W_1\left(\mu, q, \omega\right)\sin\left(\phi\right) + W_2\left(\mu, q, \omega\right)\sin\left(2\phi\right), \tag{7}$$

where $\nu = 1-\mu$; ϕ is the CB's phase when the particle is at pericenter; and the coefficients W_1 and W_2 are given by

$$W_1\left(\mu, q, \omega\right) \simeq \mu\nu(\nu-\mu)2^{1/4}\pi^{1/2}\omega^{5/2}q^{-1/4}\exp\left(-\frac{2^{3/2}}{3}\omega q^{3/2}\right), \tag{8}$$

$$W_2\left(\mu, q, \omega\right) \simeq -\mu\nu 2^{15/4}\pi^{1/2}\omega^{5/2}q^{3/4}\exp\left(-\frac{2^{5/2}}{3}\omega q^{3/2}\right), \tag{9}$$

where ω is measured in units of critical ω_0.

One may see that, at $\mu \sim 1/3$, $\omega \sim 1$, and $q \sim 2$–3, the coefficients W_1 and/or W_2 are of order unity. The normalized single-kick energy variation is ~ 1, and, therefore, indeed, an orbiting chaotic particle can be ejected in a few kicks.

In Figs. 5 and 6, the depopulation process is illustrated in detail, featuring several pre-merger phases of Arrokoth. In Fig. 6, the time dependences of the number of particles that are ejected (or collide with the CB) are shown.

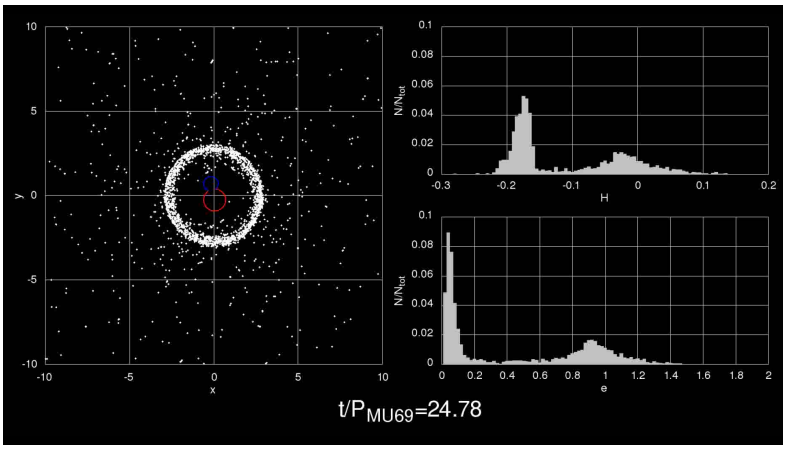

Figure 5: Simulation (video) of the depopulation process of a swarm of 10000 particles which are initially distributed in circular orbits inside a ring $[1d, 3d]$ around Arrokoth (in the post-merger phase, for the parameters obtained according to Fig. 1 in Cheng et al. (2019); here $\mu = 0.28$ and $\omega = 0.59$); H is measured in the barycentric reference frame. The video can also be found at http://perso.utinam.cnrs.fr/~lages/datasets/MU69/MU69.mp4.

The time is counted in CB's rotations. In these simulations, 10000 particles in initially circular orbits ($e = 0$) are initially uniformly distributed in a ring with $q \in [1d, 3d]$. In Fig. 6, the black curves are for the post-merger phase, where $d = d_0 = 17.2$ km, the radius of m_1 is $r_1 \simeq 10.1$ km $\simeq 0.59d$ (at which the collisions are fixed), the radius of m_2 is $r_2 \simeq 7.3$ km $\simeq 0.42d$ (at which collisions are fixed), the Hill radius is $R_{\rm H} \simeq 48740$ km $\simeq 3027d$ (at which the ejections are fixed). The observational data are taken as given in Stern et al. (2019); McKinnon (2020). The rotation period of Arrokoth is $P = 15.92$ h; this gives $\omega = 0.77\omega_{2b}$, where ω_{2b} is for the Keplerian motion. For the post-merger phase, the complete process of depopulation is visualized in the video provided in Fig. 5. Note that on timescales t greater than $\sim 100 P_{\rm MU69}$ the remaining particles are those initially trapped inside the stability islet located around $(q = 2.5, e = 0)$ in the phase space (the blue islet in Fig. 2). The red curves in Fig. 6 correspond to a pre-merger phase with $d = 3d_0 = 51.6$ km, $r_1 \simeq 10.1$ km $\simeq 0.2d$, $r_2 \simeq 7.3$ km $\simeq 0.14d$, $R_{\rm H} \simeq 821d$, $P = 63.5$ h; $\omega = \omega_{2b}$. The green curves correspond to a different pre-merger phase with $d = 5d_0 = 86$ km, $r_1 \simeq 10.1$ km

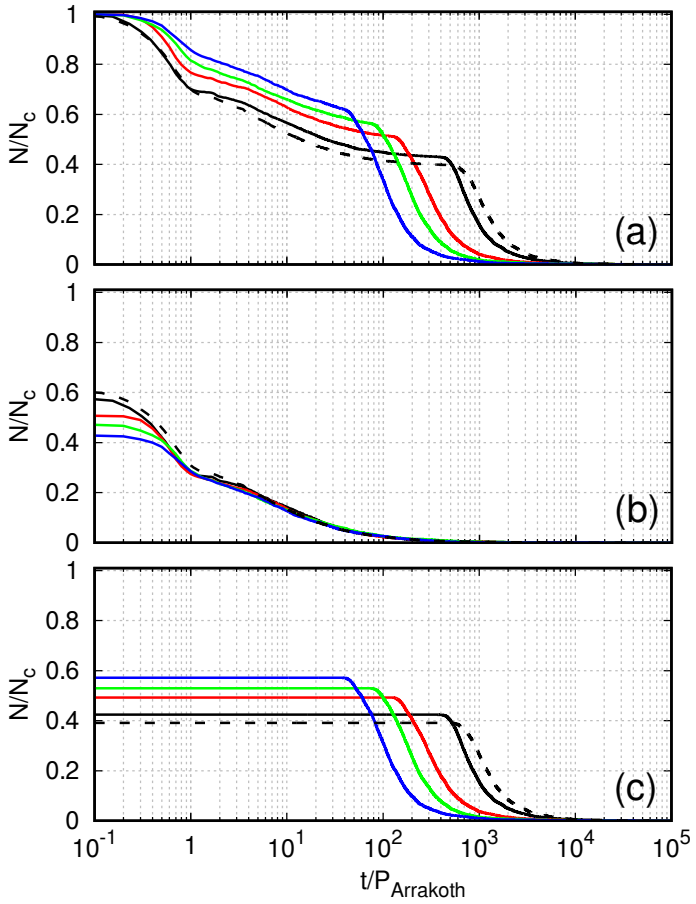

Figure 6: The number of particles ejected (or colliding with the CB) in dependence on time (counted in number of CB's rotations). Here, N_c is the number of particles initially present in the chaotic area (particles which can exit, see Fig. 2 and Fig. 3). For each panel, the black dashed line shows results for the Arrokoth parameters obtained according to Fig. 1 in Cheng et al. (2019).

$\simeq 0.12d$, $r_2 \simeq 7.3$ km $\simeq 0.08d$, $R_{\rm H} \simeq 492d$, $P = 136.6$ h; $\omega = \omega_{2b}$. The blue curves correspond to a different pre-merger phase with $d = 10.1d_0 = 172$ km, $r_1 \simeq 10.1$ km $\simeq 0.06d$, $r_2 \simeq 7.3$ km $\simeq 0.04d$, $R_{\rm H} \simeq 246d$, $P = 386.5$ h; $\omega = \omega_{2b}$.

Panel Fig. 6a represents a sum of panels (b) and (c); whereas in panel (b) the number of particles before their collision with one of CB's components is shown. In panel (c), statistics of particles before their ejection out from the Hill sphere

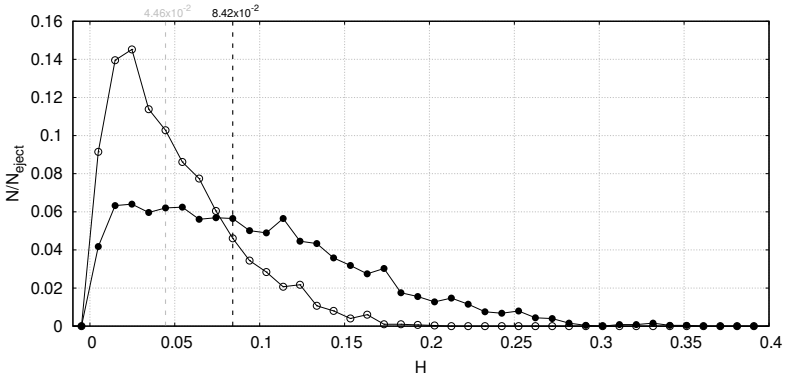

Figure 7: Black dots: the distribution of H for particles crossing the Hill sphere $R_{\rm H}$ of Arrokoth. Circles: results obtained using the Arrokoth parameters as given in Fig. 1 in Cheng et al. (2019).

are illustrated. From Fig. 6, one may infer that the depopulation process is rather fast already at the pre-merger phases of the Arrokoth formation. Indeed, in Fig. 6(c), we see that after $t \in [100, 1000]$ rotations of the binary, at least half of particles present around Arrokoth are ejected out from the Hill sphere.

By inspecting the distribution of energy when the particles leave the Hill sphere, one may calculate their "final" velocity value reached upon the ejection from the Hill sphere. In Fig. 7, the distribution of the energy H on particles' crossing Arrokoth's Hill sphere ($R_{\rm H} \simeq 42370$ km) is shown in the post-merger phase. Here, in our units, where $d = 1$, is the primaries' separation and $P_{2b} = 2\pi$ is the binary's period, $H_{1/2} \simeq 0.08$, where the first half of the ejected particles' population has $H > H_{1/2}$ and the second half has $H < H_{1/2}$. With the previous energy, the free particles reach $R_{\rm H}$ in $R_{\rm H}\omega/(2\pi\sqrt{2H_{1/2}}) \simeq 750$ rotations of Arrokoth. Indeed, by associating these findings with the results given in Fig. 6, one may conclude that the positive value of energy is reached very fast and we see that the depopulation of the CB's disk proceeds with the typical half-depopulation time (for the whole disk) ∼10–100 CB's periods, in accord with our analytical estimate given above.

In Fig. 8, the mass parameter dependence for the depopulation time $t_{H>0}$ is shown. At each separate μ value in the given range, the orbital evolution of

10^4 particles is simulated. For the orbits, the initial e is set to zero and the initial q values are set uniformly in the interval $q \in [1d, 3d]$. Any particle is regarded as ejected, if its energy H becomes positive. The depopulation time $t_{H>0}$ is fixed, when the number of particles remaining non-ejected becomes less than 1% of the initial number of particles. One may observe that, in the given range $0.1 \leq \mu \leq 0.5$, the depopulation time depends on μ rather weakly, and the depopulation process is always fast.

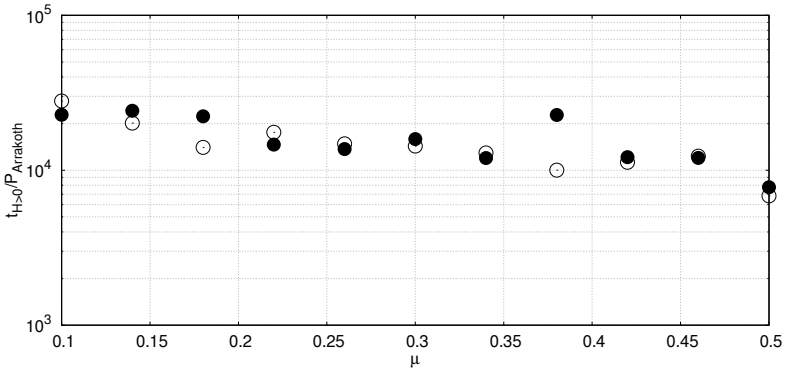

Figure 8: Black dots: the mass parameter dependence for the depopulation time $t_{H>0}$. Circles: results obtained using the Arrokoth parameters as given in Fig. 1 in Cheng et al. (2019).

6. "Mixer bowls," cocoons, and their long-term survival

As we have seen above, a rotating CB is a kind of a "cosmic mixer," efficiently dispersing any neighbouring material outwards. It is well known that any mixer (blender, eggbeater) needs a container (a bowl) to hold the ingredients from dispersal while mixing. Our cosmic mixer also needs such a storage bowl, otherwise the cocoon of matter inside its Hill sphere would not emerge.

Let us estimate the typical time $T_{\rm enc}$ between encounters of relatively large KBOs (with mass or size greater than that of Arrokoth) with Arrokoth's Hill sphere. Such low-velocity encounters would disperse Arrokoth's cocoon, if it were present. Therefore, if $T_{\rm enc}$ is much less than the Solar system age, one can be confident that the Arrokoth's Hill sphere is totally cleansed.

Let N_0 be the total number of impactors with size (radius) greater than radius R_0. Taking Arrokoth's radius for R_0, the characteristic (average) time between encounters of such KBOs with Arrokoth can be written, following a general approach of Parker & Kavelaars (2012), as

$$T_{\rm enc} = (P_{\rm i}\sigma N_0)^{-1}, \tag{10}$$

where $P_{\rm i}$ is the intrinsic collision probability, measured in km^{-2} yr^{-1}, σ is the collisional cross section, measured in km^2. For the probability $P_{\rm i}$ inside the classical Kuiper Belt, there exists two estimates: according to Farinella et al. (2000), $P_{\rm i} = 1.3 \cdot 10^{-21}$, and, according to Dell'Oro et al. (2001), $P_{\rm i} = 4 \cdot 10^{-22}$ km^{-2} yr^{-1}.

According to Equation (18) in Parker & Kavelaars (2012), number N_0 of KBOs with size $R > R_0$ can be estimated using the power-law scaling

$$N_0 = 618\,000 \cdot (26/R_0)^{q-1}, \tag{11}$$

where radius R_0 is in kilometers, and we set $q \simeq 3.5$ (a collisional equilibrium slope). With Arrokoth's $R_0 \approx 16$ km, one has $N_0 \simeq 2.1 \cdot 10^6$.

For the collisional cross section we take the cross section of Arrokoth's Hill sphere: $\sigma \simeq \pi R_{\rm H} \sim 10^{11}$ km^2. From Equation (10) one finally has $T_{\rm enc} \sim$ 4000 yr (using $P_{\rm i}$ from Farinella et al. 2000) or $T_{\rm enc} \sim 12\,000$ yr (using $P_{\rm i}$ from Dell'Oro et al. 2001).

In the both cases, $T_{\rm enc}$ is much less than the Solar system age. However, we have not yet taken into account that for an encounter to disperse the cocoon, the impact velocity should be small enough.[3] The corresponding low-velocity threshold can be specified as the velocity at which the typical time of traversing Arrokoth's Hill sphere by an impactor is about the same as the typical orbital-period timescale of particles inside the Hill sphere. If impactor's velocity is

[3] Paradoxically, for encounters between KBOs themselves, an encounter is destructive if the impact velocity is, on the opposite, high enough.

much greater than this limit, then the cocoon remains practically unperturbed.

As derived in the previous Section, the typical orbital-period timescale of particles inside the Hill sphere can be estimated as ~ 500 yr. Given the radius of the Hill sphere $R_{\rm H} \sim 5 \cdot 10^4$ km, the low-velocity limit for an impactor is then $v_{\rm cr} \sim 10^{-4}$ km/s. According to Farinella et al. (2000) (Table 1) or Dell'Oro et al. (2001) (Table 4), the mean impact velocity in the Kuiper belt is about 1 km/s. Therefore, the probability of an impact with $v < v_{\rm cr}$ is much smaller than the intrinsic impact probability. But by what amount? As follows from Dell'Oro et al. (2001) (Fig. 7), one may assume that the frequency of impacts at small and moderate v rises with v approximately linearly (for the non-resonant population) almost up to the maximum corresponding to the typical $v \sim 1$ km/s. Therefore, very roughly, one may estimate that the impacts with $v < v_{\rm cr}$ occur $\sim 10^4$ times less frequently than the typical ones. As derived above, the timescale for typical impacts is $\sim 10^4$ yr; therefore, for the dispersive low-velocity impacts the timescale is $\sim 10^8$ yr. It is still smaller than the age of the Solar system, but not dramatically.

Counting from the Solar system early epoch, Arrokoth's cocoon could have suffered $\sim$ 10–100 dispersal events; therefore one may expect that Arrokoth's Hill sphere (as well as Hill spheres of similar KBOs) nowadays is empty. However, due to a number of model approximations made, this conclusion should be subject to verification in massive numerical simulations. In particular, it should be taken into account that, at the Kuiper belt peripheral regions, where the concentration of objects can be radically less, cocoons may hypothetically survive; but this should be checked in realistic simulations.

7. Survival of space probes

Let us consider in a more detail the problem of survival of space probes visiting Arrokoth and similar objects, in the light of the analysis performed above.

Mass $m_{\rm dm}$ of the debris matter left from the formation of a given KBO is

generally expected to be less than the KBO's final mass (Umurhan et al., 2019; McKinnon et al., 2019). Therefore, for Arrokoth, $m_{\rm dm} < 2 \cdot 10^{15}$ kg. The total volume of Arrokoth, given that $R_1 \approx 10$ km, $R_2 \approx 7$ km, is $\sim 4(R_1^3 + R_2^3) \sim 5000$ km^3.

Estimating rather formally, this material, if dispersed into boulders with size of $R_b \sim 10$ cm each, would provide $\sim 10^{15}$ boulders. When mixed inside the Hill sphere (with $R_{\rm H} \sim 5 \cdot 10^4$ km), the boulder concentration would be $\rho_b \sim 10^{-16}$ cm^{-3}.

In projection on a plane, this would typically result in the column concentration $\sigma_b \sim R_{\rm H}\rho_b \sim 10^{-6}$ cm^{-2}. Given the New Horizons dimensions $2.2 \times 2.1 \times 2.7$ m, the probe cross-section is $\sim 6 \cdot 10^4$ cm^2. We see that if all the dispersed material were "conserved in the bowl," the probability of collisional destruction of the space probe would be rather significant, up to 10%. Taking smaller sizes for the dispersed boulders would raise the probability up to unity. Since New Horizons flied away safely, one may argue that the post-formation debris had already leaked from the "bowl", or there were not much of them from the very beginning.

Of course, this approach is strictly formal; first of all, a realistic size distribution for fragments should be used in our calculations. However, as soon as any realistic distribution is a power law with the power-law index ~ -3, this improvement would only produce more fragments with approximately the same total mass; therefore, the collisional probability would only aggravate.

8. Conclusions

In this article, we have explored properties of the long-term dynamics of particles (moonlets, fragments, debris or particles) around Arrokoth, as a prototype of many similar (dumbbell-shaped) objects potentially present in the Kuiper belt. The chaotic dynamics of particles inside the Hill sphere of Arrokoth (or, generally, a similar object) has been studied numerically, by means of construction of the LCE diagram, as well as analytically.

In the both numerical and analytical parts of our work, we have obtained the following results.

(1) The clearing process of the chaotic circumbinary zone is practically instantaneous: the zone is cleared in a few "kicks" of the central CB.

(2) In the studied mass parameter range $0.1 \leq \mu \leq 0.5$, the depopulation time depends on μ rather weakly, and the depopulation process is always fast, although it has a diffusive character.

(3) Due to relatively frequent low-velocity encounters of Arrokoth's Hill sphere with other KBOs, the matter cocoon, if formed inside the Hill sphere, could have been dispersed on a timescale of $\sim 10^8$ yr.

(4) If not dispersed, such a cocoon matter may pose a serious problem for the survival of any space probe visiting Arrokoth, since the collision probability could be well of order unity.

Our study has an implication concerning formation scenarios of contact binaries in the Kuiper belt. As noted in (Umurhan et al., 2019), any such scenario, apart from producing a slowly rotating CB, should treat how all remaining local debris are cleared away. We underline that, irrespective of the formation scenario, the generic chaotization of the immediate vicinities of any gravitating "snowman" rotator, followed by transport processes inside its Hill sphere, naturally explains the current absence of such debris.

Tantalizingly, the chaotic-clearing phenomenon affects both former targets of the New Horizons mission, but in different ways: Pluto is not able to clean-up any radial neighbourhood of its orbit, and on this reason it was deprived of the planetary status (IAU General Assembly, 2006); conversely, Arrokoth is able, as we have seen above, to create a clearing, but of another (circum-contact-binary) kind.

This study is a first approach to the problem. The limitations of our dynamical model include, in particular, non-taking into account the effects due to the irregular shape of Arrokoth's components on the orbiting particles, especially important for particles with small pericentric distances. (However, note that such particles, those with $q \lesssim 2d$, are absorbed by Arrokoth almost imme-

diately.) Besides, the solar gravitational effects on particles with large orbital semimajor axes (comparable with Arrokoth's Hill radius) can be important, although not many particles acquire large elliptic orbits around Arrokoth; they are mostly thrown out from its Hill sphere in a single or only several kicks (see Figs. 4 and 6). The 3D study of the escape process is envisaged, and, in the forthcoming separate study, the solar perturbations will be taken into account.

Acknowledgments. The authors are grateful to Benoît Noyelles for helpful remarks. I.I.S. was supported in part by the grant 13.1902.21.0039 of the Ministry of Science and Higher Education of the Russian Federation.

References

References

Benecchi, S. 2016. "The lightcurve of New Horizons encounter TNO 2014 MU69." HST Proposal id. 14627. Available at: http://archive.stsci.edu/

Cheng, A. F., et al. 2019. 50th Lunar and Planetary Science Conference 2019 (LPI Contrib. No. 3273)

Dell'Oro, A., Marzari, F., Paolicchi, P., & Vanzani, V. 2001. *Astron. Astrophys.*, **366**, 1053

Duncan, M., Quinn, T., & Tremaine, S. 1987. *Astron. J.*, **94**, 1330–1338

Duncan, M., Quinn, T., & Tremaine, S. 1989. *Icarus*, **82**, 402–418

Farinella, P., Davis, D., & Stern, S. 2000, in Protostars and Planets IV, ed. V. Mannings, A. Boss, & S. Russell (Tucson, AZ: Univ. Arizona Press), 1255

Gladstone, G. R., et al. 2019. 50th Lunar and Planetary Science Conference 2019 (LPI Contrib. No. 2866)

Hairer, E., Nørsett, S.P., & Wanner, G. 1987. Solving Ordinary Differential Equations I. Nonstiff Problems (Springer-Verlag, Berlin)

IAU 2006 General Assembly: Result of the IAU Resolution votes 2006. IAU0603 – Press Release. Available at: http://www.iau.org/news/pressreleases/detail/iau0603/

Kammer, J., et al. 2018. *Astron. J.*, **156**, 72 (7pp)

Lages, J., & Shevchenko, I. I. 2020. In: *Origins: From the Protosun to the First Steps of Life* (Proc. IAU Symp. 345), ed. by Elmegreen, B. G., Viktor Tóth, L., & Güdel, M. (Cambridge Univ. Press, Cambridge) pp. 227–229

Lages, J., Shepelyansky, D. L., & Shevchenko, I. I. 2017. *Astron. J.*, **153**, id. 272

Lages, J., Shepelyansky, D. L., & Shevchenko, I. I. 2018. *Scholarpedia*, **13(2)**:33238

Lages, J., Shevchenko, I. I., & Rollin, G. 2018. *Icarus*, **307**, 391–399

Malyshkin, L., & Tremaine, S. 1999. *Icarus*, **142**, 341–353

McKinnon, W. B., et al. 2019. 50th Lunar and Planetary Science Conference 2019 (LPI Contrib. No. 2767)

McKinnon, W. B., et al. 2020. *Science*, 10.1126/science.aay6620

Meiss, J. D. 1992. *Rev. Mod. Phys.*, **64**, 795

Moore, J. M., et al. 2018. *Geophysical Research Letters*, **45**, 8111–8120

Morrison, S., & Malhotra, R. 2015. *Astrophys. J.* **799**, 41

Murray, N., & Holman, M. 1997. *Astron. J.*, **114**, 1246–1259

Nesvorný D. et al. 2018. *Astron. J.*, **155**, 246

Parker, A. H., et al. 2017. "Multiplicity of the New Horizons extended mission target (486958) 2014 MU69." 49th Meeting of the AAS Division for Planetary Sciences. Abstract 504.04

Parker, A. H., & Kavelaars, J. J., 2012. *Astrophys. J.*, **744**, 139 (14pp)

Protopapa, W. M., et al. 2019. 50th Lunar and Planetary Science Conference 2019 (LPI Contrib. No. 2732)

Scheeres, D. J., 2007. *Icarus*, **189**, 370–385

Shao, Y., & Lu, H. 2000. *J. Geophys. Res.*, **105**, 22437–22443

Shevchenko, I. I. 2011. *New Astronomy*, **16**, 94–99

Shevchenko, I. I. 2015. *Astrophys. J.*, **799**, 8

Shevchenko, I. I., & Melnikov, A. V. 2003. *JETP Letters*, **77**, 642 [*Pis'ma ZhETF*, **77**, 772]

Spencer, J. R., et al. 2019. 50th Lunar and Planetary Science Conference 2019 (LPI Contrib. No. 2737)

Spencer, J. R., Stern, S. A., Moore, J. M., Weaver, H. A., Singer, K. N., et al. (2020) "The geology and geophysics of Kuiper Belt object (486958) Arrokoth." Science, 10.1126/science.aay3999 (19pp)

Stern, A. 2017. "The PI's Perspective: The Heroes of the DSN and the 'Summer of MU69'. (August 8, 2017.)" Available at: http://pluto.jhuapl.edu/News-Center/

Stern, S. A., et al. 2019. 50th Lunar and Planetary Science Conference 2019 (LPI Contrib. No. 1742)

Stern, S. A., Weaver, H. A., Spencer, J. R., Olkin, C. B., Gladstone, G. R., et al. (2019) "Initial results from the New Horizons exploration of 2014 MU69, a small Kuiper Belt object." Science, **364**, eaaw9771 (12pp)

Thirouin, A., Noll, K. S., Ortiz, J. L., & Morales, N. 2014. *Astron. Astrophys.*, **569**, A3

Thomas, N., et al. 2015. *Astron. Astrophys.*, **583**, A17

Tremaine, S. 1993. In Phillips J.A., Thorsett J.E., Kulkarni S.R., eds, Planets Around Pulsars, ASP Conf. Series, **36**, 335–344

Umurhan, O. M., et al. 2019. 50th Lunar and Planetary Science Conference 2019 (LPI Contrib. No. 2809)

Wisdom, J. 1980. *Astron. J.*, **85**, 1122–1133